



ELSEVIER

Available online at www.sciencedirect.com

SCIENCE @ DIRECT®

Icarus ●●● (●●●●) ●●●—●●●

ICARUS

www.elsevier.com/locate/icarus

# Determination of the meteoroid velocity distribution at the Earth using high-gain radar

S.M. Hunt,<sup>a,b,\*</sup> M. Oppenheim,<sup>b</sup> S. Close,<sup>a,b</sup> P.G. Brown,<sup>c</sup> F. McKeen,<sup>a</sup> and M. Minardi<sup>d</sup>

<sup>a</sup> MIT Lincoln Laboratory, Lexington, MA 02420-91008, USA

<sup>b</sup> Boston University, Boston, MA 02215, USA

<sup>c</sup> University of Western Ontario, London, ON, Canada

<sup>d</sup> Wright State University, Dayton, OH 45435, USA

Received 4 March 2003; revised 4 August 2003

## Abstract

Plasma formed in the immediate vicinity of a meteoroid as it descends through Earth's atmosphere enables high-gain radars such as those found at Kwajalein, Arecibo, and Jicamarca to detect ablating meteoroids. In the work presented here, we show that these head echo measurements preferentially detect more energetic meteoroids over less energetic ones and present a method of estimating the effects of this bias when measuring the velocity distributions. To do this, we apply ablation and ionization models to estimate a meteoroid's plasma production rate based on its initial kinetic energy and ionization efficiency. This analysis demonstrates that, almost regardless of the assumptions made, high-gain radars will preferentially detect faster and more massive meteoroids. Following the model used by Taylor (1995, *Icarus* 116, 154–158), we estimate the biases and then apply them to observed meteoroid velocity distributions. We apply this technique to observations of the North Apex meteoroid source made by the Advanced Research Project Agency Long Range Tracking and Instrumentation Radar (ALTAIR) at two frequencies (160 and 422 MHz) and compare results from the Harvard Radio Meteor Project (HRMP) at High Frequency (HF, 40.9 MHz). Both studies observe a peak in the distribution of North Apex meteoroids at approximately  $56 \text{ km s}^{-1}$ . After correcting for biases using Taylor's method, the results suggest that the mass-weighted peak of the distribution lies near  $20 \text{ km s}^{-1}$  for both studies. We attribute these similarities to the fact that both radar systems depend upon similar ablation and ionization processes and thus have a common mass scale.

© 2003 Published by Elsevier Inc.

*Keywords:* Meteoroid velocity distribution

## 1. Introduction

High-gain radars have sufficient sensitivity to detect plasma created at the head of a meteoroid's path during its atmospheric descent. Meteor head echoes were first observed using a VHF (65 MHz, 4.6 m wavelength) radar by Hey et al. (1947). In the last decade, head echo measurements made by narrow-beam, high-power radar systems have been applied to meteor astronomy. The high sensitivity and resolution of these systems enables the collection of high-quality data (Fig. 1), which provides the direction of origin, velocity, and deceleration of a meteoroid (Close et al., 2000; Hunt et al., 2001; Janches et al., 2000a, 2000b; Mathews et al.,

1997; Pellinen-Wannberg and Wannberg, 1994; and Zhou et al., 1998).

This paper presents a study of the nature and effects of the biases inherent in using head echoes to determine the velocity distribution of meteoroids entering Earth's atmosphere. Since head echo measurements result from radio wave reflection off electrons subsequent to meteoroid mass ablation and ionization, meteoroids that produce the greatest number of electrons often create the strongest signal returns. The meteoroid body itself is too small (radius  $\sim 10^{-6}$  m) to be detected. We study the detection process by modeling the production of ionization for a meteoroid with a given initial mass and velocity. We show that, almost regardless of the assumptions made, high mass and high-velocity meteoroids will produce strong head echo reflections while slower, less massive meteoroids will produce so little ionization that radar cannot detect a head echo. We present data from the

\* Corresponding author.

E-mail address: hunt@ll.mit.edu (S.M. Hunt).

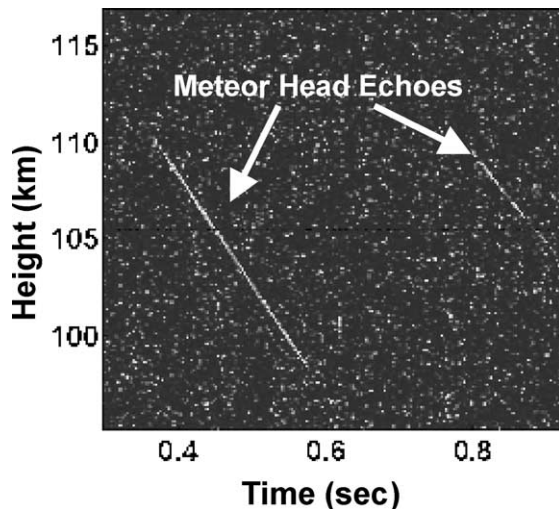


Fig. 1. Range-time-intensity image of ALTAIR VHF head echo data. These data are an example of unprocessed digital samples used to determine meteor head echo parameters. They were collected using ALTAIR during the 1998 Leonid meteor shower at the equatorially located Reagan Test Site.

ALTAIR radar corroborating this picture. We then apply the techniques used by Taylor (1995) to approximate and correct for the bias in velocity distributions from HRMP meteor trail observations to ALTAIR head echo observations.

Both systems show a measured North Apex distribution peak near  $\sim 56 \text{ km s}^{-1}$ . The application of the techniques used to estimate the observational biases, suggests that the mass-weighted peak actually resides near  $15\text{--}20 \text{ km s}^{-1}$  for both datasets. While these two radars use substantially different techniques to estimate the velocity of meteoroids, the biases appear quite similar due to the physics of meteor ionization which is dependent on meteoroid kinetic energy (Hawkins, 1956). We conclude by arguing that high-gain radars detect a greater segment of the meteoroid population than the low gain specular trail meteor radars, but these observations are similarly biased by the physics of ionization production and radar sensitivity.

Section 2 provides background on radio meteor observation, physics and biases. Section 3 describes observations made with the ARPA Long Range Tracking and Instrumentation Radar (ALTAIR), and the Harvard Radio Meteor Project (HRMP) system. Section 4 outlines the techniques used to determine meteor velocity from meteor trail and head echo data. Section 5 compares modeled meteor line density with values measured by high-gain radars. Section 6 presents the bias correction technique and applied it to observations made by the high-gain ALTAIR radar.

## 2. Radio meteors

As meteoroids enter Earth's atmosphere, they are heated by collisions with atmospheric constituents. The rate at which collisions take place depends upon a meteoroid's physical cross-section, velocity and atmospheric density

(Opik, 1958). Therefore, faster meteoroids heat more quickly because they undergo a greater number of collisions per unit time. The collisional processes include grazing surface impacts, which scatter material, and surface penetration of the meteoroid body by impinging air particles, which increases the meteoroid's thermal temperature (Whipple, 1950). The initial meteoroid mass and velocity, prior to atmospheric entry, determine the amount of kinetic energy available for the creation of heat, light and ionization. Other sources of energy, such as Earth's gravity, are negligible by comparison.

Early on, most radar observations of meteoroid plasma were collected with low frequency Yagi antenna systems, such as the one used for the HRMP (VHF-40.92 MHz, 7.3 m wavelength). Unlike head echoes, these observations are based on specular reflection from large segments ( $\sim$  few kilometers) of the ionized meteor trail (Baggaley et al., 1994). These observations typically have higher signal detection thresholds and lower spatial resolution than high-gain radar head echo observations. Therefore, most early radio-meteor observations consisted of specular meteor trail echoes. These only occur when the radar line of sight is oriented perpendicular to the flight path of a meteoroid. Under ideal conditions, the ionization trail behind a meteor reflects in phase along a large segment of the trail, producing large returns making high signal-to-noise meteor trail observations possible.

The spatial distribution of meteor plasma and the size of the incident radar wavelength determine the radar wave reflection coefficient (Close et al., 2003). Specular radar trail observations become attenuated at heights where the initial trail radius, corresponding to some multiple of the atmospheric mean free path, becomes roughly the same or greater than the radar wavelength. This sets a maximum height, called the meteor ceiling, where meteors can be easily observed using specular radar (Cepelcha et al., 1998).

The contributions of the radio meteor detection bias can be separated into components of initial mass and velocity (Bronshen, 1983; Taylor, 1995). The mass of each meteoroid is unknown and therefore can only be bounded by a minimum detectable value (for each velocity), dependent on radar sensitivity. The observational velocity bias is a function of the ionization efficiency,  $\beta$  (Jones, 1997).  $\beta$  is defined as the fraction of neutral atoms that travel at velocity,  $V$ , that will ionize. Experiments and theory show that  $\beta$  scales as a power of  $V$ ,  $\beta \propto V^\gamma$ , where  $\gamma$  spans approximately 3.0–5.50 (Bronshen, 1983). Both specular trail and head echo observations are affected by this dependence of ionization production on velocity.

The detection rate of radio meteors depends upon the

- (1) density and spatial distribution of the meteoroid plasma coupled with the corresponding radio-signal reflection processes,
- (2) radar sensitivity, and
- (3) radiant distribution of sporadic meteors.

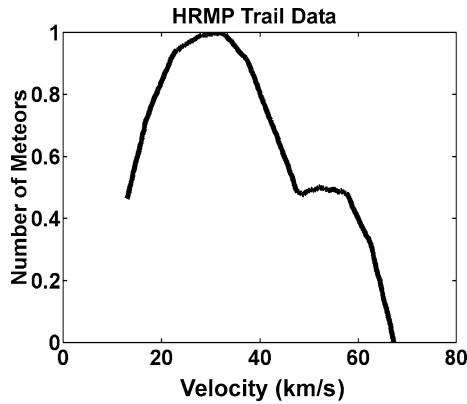


Fig. 2. Observed HRMP meteor velocities from meteor trail measurements obtained during the 1968–1969 synodic year.

Factor 3 relies on the fact that the flux contribution of shower meteors distributed across the celestial sphere is small relative to the sporadic population.

Taylor (1997, 1998) identified the radiant distribution of sporadic meteors from bias-corrected HRMP observations. Jones and Brown (1993) analyzed radar and optical surveys of the sporadic background and reconciled a consistent multi-frequency view of the sporadic distribution with greater detail. They found the sporadic meteoroid background seen at Earth consisted of six major sources, symmetric about the ecliptic plane. Each source had a particle population with its own characteristic distribution of orbital elements. The relative apparent strength of these sporadic sources was further examined by Brown and Jones (1995), who found that the helion and anti-helion source contributed 33% (each) of the sporadic flux, the North and South toroidal source contribute 5% (each), with the remainder due to the Apex sources. Taylor breaks the distribution of the sporadic meteor population into the following components (weighted by mass): helion (33%), anti-helion (36%), North Apex (4%), South Apex (4%), North toroidal (6%), and South toroidal (6%). The remainder of the sporadic meteor population originates from regions in between these apparent sources. Figure 2 illustrates the HRMP meteor trail observations ( $\sim 14,000$ ) from all of these sources taken during the 1968–1969 synodic year. The dominant contribution from the slower moving helion and anti-helion meteor sources determine the peak of the apparent distribution near  $32 \text{ km s}^{-1}$ .

### 3. Observations

The ALTAIR and HRMP systems offer different capabilities for application to radio meteor astronomy. This section outlines basic features of both systems. The application of ALTAIR to meteor astronomy (Close et al., 2000) is relatively new. The HRMP system characteristics are covered by Hawkins (1963).

ALTAIR is one of several observing systems located at the Reagan Test Site (RTS) on the Kwajalein Atoll ( $9^\circ \text{ N}$ ,  $167^\circ \text{ E}$ ) in the Republic of the Marshall Islands. ALTAIR has a 43-m diameter, mechanically steered, parabolic dish and simultaneously transmits a peak power of 6 MW at two-frequencies (VHF-160 MHz, 1.86 m wavelength, UHF-422 MHz, 0.71 m wavelength). We used a 10 dB signal-to-noise (S/N) ratio to identify head echo detections. The ALTAIR observations presented here are enriched in faster moving North Apex meteoroids. North Apex particles are primarily in retrograde solar orbits, causing their observed velocities to be near  $60 \text{ km s}^{-1}$  (Brown et al., 2001). Using the most sensitive waveforms available, ALTAIR can detect radar cross-sections (RCS) as small as  $-74$  decibels-relative-to-a-square-meter (dBsm) at VHF ( $-80$  dBsm at UHF) at a range of 100 km (Close et al., 2000). A target with a RCS of 100 square meters is equivalent to 20 dBsm on a logarithmic scale.

Rigorous calibration procedures executed at ALTAIR maintain the range, angle and RCS measurement accuracy of the system. The details and frequency of the calibration procedure will not be covered here. The ALTAIR system accuracy relative to a known independent source bounds the expected accuracy of the measured results (Coster et al., 1992; Hunt et al., 2000). ALTAIR measurement errors going back to 1983 show stable average rms tracking errors relative to the precision orbits for earth orbiting satellites of (i.e., Experimental Geophysical Payload) of  $\pm 15$  milli-degrees in angle and  $\pm 6$  m in range (Hunt et al., 2000). The meteor head echo analysis of ALTAIR data show that the fit error in angle and range are of comparable magnitude. ALTAIR is also calibrated to the RCS of a known target, a uniform 22-inch aluminum sphere; the absolute RCS measurement capability of ALTAIR is  $\pm 0.5$  dB.

We collected ALTAIR meteor observations on November 18, 1998 during a 4-hour period chosen to span the predicted peak of the Leonid shower (07:30 AM local time). The peak detection rate reached approximately 1 head echo every 2 seconds. ALTAIR did not detect any Leonids meteors. Statistically, the likelihood of detecting stream meteors with narrow-beam high-gain radar is very small. Analysis of this head echo detection rate shows that it equates to a minimum detectable visual meteor magnitude of  $+11$  at UHF and  $+12$  at VHF (Brown et al., 2001). The radar sample window encompassed slant-ranges corresponding to heights spanning 70 to 140 km at VHF and 90 to 110 km at UHF. We used  $40 \mu\text{s}$  (VHF) and  $150 \mu\text{s}$  (UHF) pulsed waveforms. The range sample spacing used to collect the majority of the data was 7.5 m at UHF and 30 m at VHF.

Linear frequency modulation (LFM) of the transmit signal coupled with pulse compression of the received signal defines the attainable range resolution. The waveform bandwidths,  $B$ , are 1 MHz (VHF) and 3 MHz (UHF). After pulse compression upon the reception of the signal, the attainable range resolution is  $(\Delta R = c/(2B))$ , where  $c$  is the speed of light. Finally we correct the meteor range for range-Doppler

coupling. Range-Doppler coupling is a property of a LFM pulse (Skolnick, 1980). A Doppler shift ( $\Delta f_{\text{Doppler}}$ ) of the transmitted LFM pulse occurs because of the observed meteor range-rate. Following pulse compression, the meteor range incurs a slight range offset that is a function of the observed range-rate. The relationship between target range rate and the range-Doppler coupling range offset is

$$\varepsilon_{\text{Range}} = \frac{cT \Delta f_{\text{Doppler}}}{B} = \frac{T f_0 v_{\text{radial}}}{B},$$

where  $\varepsilon_{\text{Range}}$  is the range offset,  $T$  is the pulse width,  $f_0$  is the radar frequency, and  $v_{\text{radial}}$  is the target radial velocity.

The HRMP specular meteor trail radar was located in Havana Illinois (40° N, 270° E) and consisted of a single transmit antenna with several Yagi receive antennas. It operated at 40.92 MHz with a peak transmit power ranging from 0.6 to 4.0 MW (Verniani, 1973). Simultaneous multi-station measurements of meteor trails enabled the determination of three-dimensional position as a function of time (Hawkins, 1963). The HRMP radar provided broad sky coverage and dedicated availability that allowed for long periods of operation. Therefore the HRMP study provided a broad spatial and temporal sample of the sporadic meteoroid population (Taylor, 1997) that revealed a non-uniform directionality to the meteoroid flux distribution at Earth. The collection of an equivalent dataset with narrow-beam high-gain radar does not yet exist.

Unlike the ALTAIR dataset, the HRMP sporadic meteor observations spanned several years and provided a more uniform sampling of the overall population. ALTAIR observations were made with the beam pointing within the North Apex meteor source, which is approximately 20 degrees in radius and centered at the longitude of the Earth's direction of motion and at approximately 30 degrees North ecliptic latitude (Jones and Brown, 1993). In this paper, HRMP North Apex meteors are analyzed to provide a sample that is consistent with the ALTAIR (North Apex) observations.

#### 4. Radio meteor velocity determination

For the HRMP observations, meteor velocity was computed from the oscillation rate measured in the received signal amplitude (Baggaley et al., 1997). As the meteor traverses the atmosphere, the signal oscillates due to changing constructive and destructive interference patterns produced by the ionized trail Fresnel zones (Cepelcha et al., 1998).

The greater sensitivity of high-gain systems (versus meteor trail radars) such as ALTAIR, Arecibo, the European Incoherent Scatter (EISCAT) radar, and Middle and Upper atmosphere (MU) radar, facilitate the calculation of meteor velocities directly from the precise range and Doppler measurements of head echoes (Close et al., 2001; Janches et al., 2000a). We use the pulse-by-pulse time rate of change of head echo position along its flight path to compute meteor velocity and apply the monopulse angular measurements to determine the meteor's three-dimensional position.

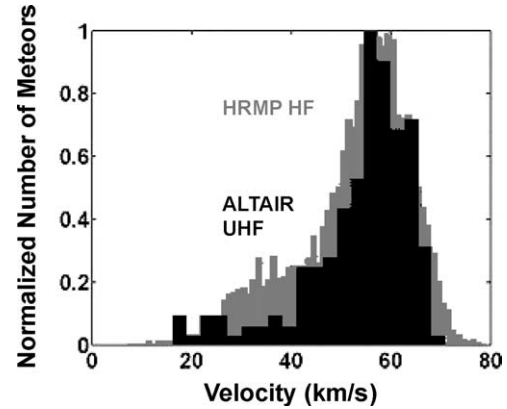


Fig. 3. Normalized number of North Apex meteors versus observed velocity from the HRMP study and ALTAIR. These data from both systems show a consistent velocity peak near  $56 \text{ km s}^{-1}$ . The HRMP results were obtained from specular meteor trail observations while the ALTAIR result was obtained from head echo measurements. These plots illustrate that the two systems provide a consistent assessment of the North Apex meteor velocity distribution. The differences in these distributions are mainly attributable to the weaker statistics of the ALTAIR head echo data ( $\sim 350$ , UHF) versus the HRMP trail observations ( $\sim 14,000$ ).

Both HRMP and ALTAIR measure a consistent velocity distribution of North Apex meteors as shown in Fig. 3. The similarity of these velocity distributions implies that both methods preferentially measure a similar high-velocity subpopulation of the total meteoroid distribution. The differences in the observations between these two radar systems arise from their differing sensitivities and velocity determination techniques, though variability in meteor ionization will likely have a far greater effect on the measured distributions.

#### 5. Modeling line density and comparison with data

This section presents two forms of single-body meteor ablation theory used to predict the maximum meteor ionization produced as a function of initial meteoroid mass and velocity. We compare these predictions with a sample of ALTAIR head echo observations and conclude from this comparison that radars measuring head echoes preferentially detect faster and more massive meteoroids. The ALTAIR radar, like all radars, has a sensitivity cutoff which precludes observations of smaller, slower meteoroids.

##### 5.1. Single-body mass ablation models

In the first model we apply single-body meteor theory developed by Opik (1958). As a meteor descends through Earth's atmosphere it encounters an air mass  $dm$  equal to  $A \rho_{\text{air}} V dt$ . Where  $A$  is the meteoroid's physical cross-section ( $\pi r_{\text{meteoroid}}^2$  for a sphere), the empirical Mass Spectrometer and Incoherent Scatter Radar (MSIS-90) atmospheric model (Hedin et al., 1983, 1987, 1991) defines the mean atmospheric mass density,  $\rho_{\text{air}}$ , and  $V$  is the veloc-

ity. Ignoring any fragmentation of the meteoroid body, this interaction causes the meteoroid to decelerate as:

$$\frac{dV}{dt} = \frac{-1}{m}(A\Gamma\rho_{\text{air}}V^2), \quad (1)$$

where  $\Gamma$  is the aerodynamic drag and  $m$  is the mass of the meteoroid at time  $t$ . Less than 10% of the ALTAIR head echo observations indicate fragmentation is taking place, therefore the assumption appears reasonable.

The meteoroid mass loss equation

$$\frac{dm}{dt} = -A\Gamma\rho_{\text{air}}\sigma_a V^3 \quad (2)$$

describes how mass is ablated as a function of time, where the ablation parameter,  $\sigma_a = 10^{-12} \text{ s}^2 \text{ cm}^{-2}$ , is taken as constant (Opik, 1958; Bronshten, 1983; Verniani, 1973). Verniani determined that the ablation parameter varied from  $10^{-10.4}$  to  $10^{-12.5}$  from the analysis of radio meteors. A value of  $10^{-12}$  corresponds to meteoroid masses of approximately  $10^{-6}$  g. This ablation parameter simplifies the characterization of how kinetic energy is converted to heat by the meteoroid and the rate at which material is ablated off the body.

The ablation parameter,  $\sigma_a$ , used with the two-equation model approximates the details of the energetic processes that define meteor ablation. A more physically detailed formulation (Whipple, 1950) later presented by Lebedinets (1973) and Grebowski (1981) is outlined here for comparison. In this three-equation model, a spherical, stony meteoroid still decelerates without fragmentation as defined by Eq. (3) but the ablation rate and temperature are now governed by a more sophisticated model.

Initially meteoroids are assumed to enter the atmosphere at an equilibrium temperature equal to the ambient background at approximately 270 degrees Kelvin (Whipple, 1951, 1966). The energy required to break the solid bonds of a gram of meteoroid substance is the latent heat of vaporization,  $Q$  (Bronshten, 1983). For this model, the aerodynamic drag,  $\Gamma$ , latent heat,  $Q$ , and the heat transfer coefficient,  $\Lambda$ , are assumed constant throughout the flight path of the meteor. The heat transfer coefficient defines the fraction of the kinetic energy per unit time,  $\text{KE} = \frac{1}{2}A\rho_{\text{air}}V^3$ , of the impinging air molecules that heat the meteoroid.

Most meteoroid kinetic energy is given off as heat; lesser amounts produce ionization and visible light (Ceplecha et al., 1998). For meteoroids approximately 1 cm and larger, the existence of an interaction layer at the front of the meteoroid will likely influence the local number density of the electrons and the corresponding signal strength observed by radar. Since meteoroids that produce the bulk of head echo detections are small relative to the mean free path of escaping meteoric atoms, no interaction layer is modeled in this analysis. The lack of an interaction layer means that meteoroid heating and the corresponding ablation is defined by individual collisions with atmospheric particles (free molecular flow).

The atmospheric collisions result in the sputtering and vaporization of meteoric atoms. Sputtering is the shedding of material from grazing surface impacts while vaporization is due to the meteoric material being raised to the heat of vaporization leading to the subsequent boiling off of individual atoms resulting in an increased mass loss rate. During the vaporization stage, meteoric particles depart the surface at the thermal velocity and subsequently collide with atmospheric particles (Whipple, 1950). For a meteoroid with an average atomic mass of 23 atomic mass units, the thermal velocity is approximately  $1-2 \text{ km s}^{-1}$ . Since the thermal speed is small relative to the speed of a meteoroid, the meteoroid speed is used for the collision speed of a meteoric atom with atmospheric particles (Ceplecha et al., 1998). The meteoroid speed defines the amount of collisional energy available to ionize meteoric and atmospheric constituents.

The meteoroid temperature as a function of time is described by the energy equation

$$\frac{dT}{dt} = -\frac{A\rho V^3}{2C_3}(\Lambda - \Lambda_S) - \frac{4A\sigma_{SB}(T^4 - T_0^4)}{C_3} - \frac{4AC_1Q}{C_3T^{1/2}}e^{-C_2/T}, \quad (3)$$

where  $T$  is the temperature of the meteoroid,  $T_0$  is its equilibrium temperature at atmospheric entry,  $\Lambda_S = Q(6 \times 10^{-16})e^{T/290}$  is the sputtering efficiency that defines the rate of ablation due to individual surface collisions. The constants appropriate for stony meteoroids are  $C_1 = 6.92 \times 10^{10} \text{ g cm}^{-2} \text{ s}^{-1} \text{ K}^{1/2}$ ,  $C_2 = 57800 \text{ K}$ ,  $C_3 = 1 \times 10^7 \text{ ergs g}^{-1} \text{ K}^{-1}$ ,  $Q = 7 \times 10^{10} \text{ ergs s}^{-1}$ , and  $\sigma_{SB} = 5.68 \times 10^{-5} \text{ ergs cm}^{-2} \text{ s}^{-1} \text{ K}^4$  (Lebedinets, 1973).

The meteoroid mass loss equation,

$$\frac{dM}{dt} = -\frac{4AC_1}{T^{1/2}}e^{-C_2/T} - \frac{\Lambda_S\rho_{\text{air}}AV^3}{2Q}, \quad (4)$$

describes how mass is ablated as a function of time. The loss rate of meteoric atoms and the ionization efficiency of each meteoric constituent determine the number of electrons produced by the meteor along its flight path.

The ablation theories estimate the loss rate of meteoric atoms. These mass loss rates, combined with an estimate of the ionization efficiency, predict the amount of the plasma detected by radar, namely the electron line density,  $q$  (Opik, 1958), of the meteor trail in electrons cm,

$$q = \frac{\beta}{M_a V} \left( \frac{dM}{dt} \right), \quad (5)$$

where  $\beta$  is the ratio of the neutral meteoric atoms (due to sputtering and vaporization) traveling at velocity,  $V$ , that will ionize (Bronshten, 1983).  $M_a$  is the mass of a typical meteoric atom.

For the purposes of the work presented here,  $\beta$  is assumed to have a  $V^\gamma$  power law dependency (Massey and Sida, 1955; Hawkins, 1956; Hawkins et al., 1964). Lebedinets (1973) value of  $\beta = \beta_0 V^{3.5}$ , where  $\beta_0 = 4.0 \times 10^{-25} (\text{cm s}^{-1})^{-3.5}$ , provides results consistent with observation

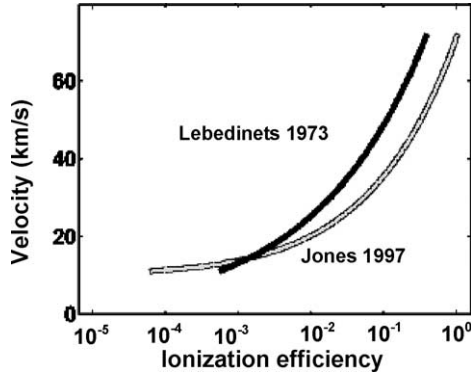


Fig. 4. Ionization efficiency from Jones (1997) and Lebedinets (1973). For the work presented here the value from Lebedinets was chosen since it provides electron line density values most consistent with ALTAIR head echo observations.

for our expected range of meteoroid masses ( $10^{-10} \text{ g} \leq m \leq 10^{-4} \text{ g}$ ) and velocities ( $11 \text{ km s}^{-1} \leq V \leq 72 \text{ km s}^{-1}$ ). For comparison, Fig. 4 illustrates values of ionization efficiency using the Lebedinets and Jones models. The Jones (1997) model of ionization efficiency,  $\beta_J = K_I(V_M - V_I^2)V_M^{0.8}$ , contains factors dependent on each meteoric constituent. In this equation,  $K_I$  is a constant,  $V_I$  is the velocity associated with the ionization energy for each meteoric species and  $V_M$  is the meteoroid velocity.

We perform numerical integration (4th order Runge-Kutta) on these single-body meteoroid ablation theories and illustrate the relation between the initial mass and velocity of meteoroids and their corresponding ionization production in Earth's atmosphere. Using a constant meteoroid mass density of  $2.5 \text{ g cm}^{-3}$  and a mass of  $10^{-4} \text{ g}$ , the results from the numerical integration of the two- and three-equation single-body ablation theory are plotted in Fig. 5.

The major dissimilarity between the two models is that the three-equation (Lebedinets, 1973) model attempts a more accurate treatment of the meteoroid temperature with height. This has a direct effect on the mass ablation rate. The meteoroid temperature, ablation rate and corresponding ionization production of the three-equation model exceeds that predicted by the two-equation model (Fig. 5).

The evaluation of the electron line density equation at the point of maximum density for each meteor provides a quantity that can be readily compared to head echo observations. A relation was first deduced by Herlofson (1948) to determine electron line density relative to the point of maximum line density along the meteoroid trajectory. Herlofson assumed an isothermal atmosphere, that the meteor parameters  $A$ ,  $\Gamma$ ,  $\sigma$ ,  $Q$ ,  $\rho_{\text{meteor}}$  are constant, and that the derivatives  $dm/dt$  and  $d\rho_{\text{air}}/dt$  are small at the point of maximum line density, such that

$$q_{\text{max}}(\rho_{\text{air}} = \rho_{\text{air max}}) \propto CM_0 V_0^\gamma, \quad (6)$$

where  $C$  is a constant,  $M_0$ ,  $V_0$  are the initial mass and velocity of the meteoroid and  $\gamma$  is the power of the ionization efficiency. This equation is derived directly from meteor ab-

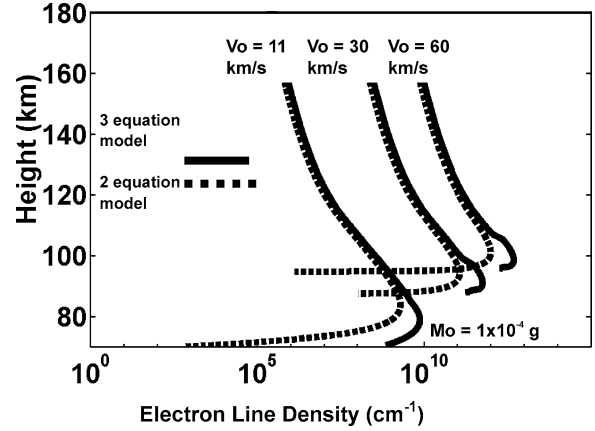


Fig. 5. Electron line density versus height above Earth for a stony micro-meteoroid ( $\rho_{\text{meteor}} = 2.5 \text{ g cm}^{-3}$ , initial mass =  $10^{-4} \text{ g}$ ). This plot contains electron line density values from the two- and the three-equation models (Section 5). The differences in the two models are attributable to the variability of ablation with temperature that exists in the three-equation model; a constant value of  $\sigma_a = 10^{-11}$  was used with the two-equation model.

lation theory and radar observations and therefore defines the physical basis of the mass and velocity bias experienced by radar. Within the approximations of single-body meteor theory, this result applies directly to both meteor head echo and meteor trail RCS observations. Conveniently, the modeled  $q_{\text{max}}$  corresponds to the point of greatest signal to noise discernable by radar head echo observations (maximum head echo RCS), which the model predicts to occur at approximately 103 km for ALTAIR VHF for meteoroids traveling at  $56 \text{ km s}^{-1}$  with masses near  $10^{-6}$  to  $10^{-4}$  grams.

### 5.2. Measured and modeled electron line density

To solve for maximum electron line density using ALTAIR head echo data, we employ a spherical three-dimensional full-wave scattering solution (Close et al., 2003). The need for a full-wave solution arises when the electric permittivity changes appreciably in one wavelength. In other words, the gradient scale size for the index of refraction is similar to the radar wavelength. In order to calculate the radio signal reflection coefficients of head echoes the plasma distribution is assumed spherical with a density that decreases exponentially with distance from the meteoroid center.

Figures 6 and 7 illustrate the modeled and observed maximum electron line density as a function of initial meteoroid mass and velocity. We compute the modeled maximum line density values by numerically integrating the three-equation mass ablation model and then selecting the maximum line density for each initial mass-velocity parameter pair. Both distributions demonstrate the dependence of maximum electron line density on velocity. The dashed line illustrates the observed detection cut off for the ALTAIR North Apex head echo observations. The ALTAIR head echo observations show little or no detections below the modeled

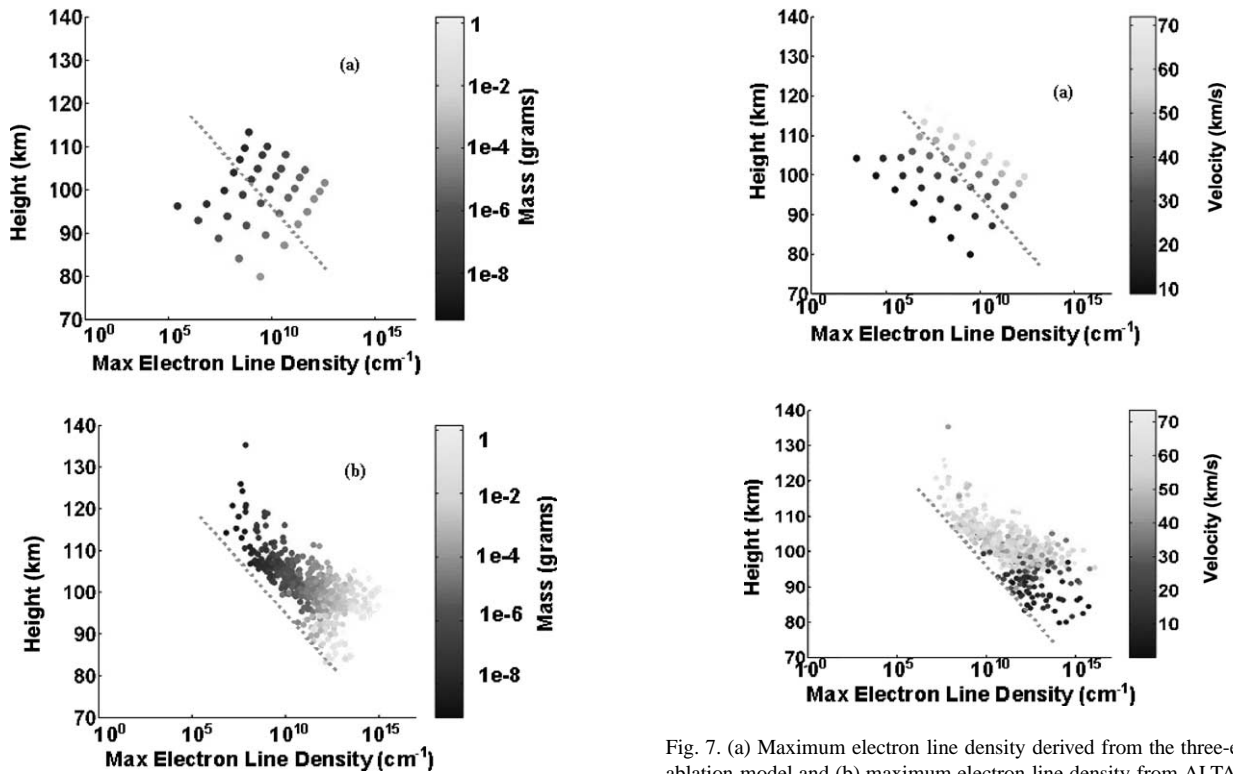


Fig. 6. (a) Maximum electron line density derived from the three-equation ablation model and (b) maximum electron line density from ALTAIR head echo observations. These data are all plotted as a function of height above earth and meteor velocity. The model results show physically consistent characteristics to the ALTAIR observations shown in (b). The dashed line illustrates the detection threshold for ALTAIR North Apex meteor observations. The maximum line density observations are obtained by the application of the 3D full-wave scattering theory to the ALTAIR RCS measurements.

micro-meteoroid ablation limit (mass threshold of  $10^{-10}$  g for stony meteoroid). The differences between the measured and modeled values are likely due to an inconsistency in the model calibration with ALTAIR. A future area of work is to better calibrate the mass ablation model using ALTAIR head echo observations.

The similarity of the model and measured distributions indicates a surprising level of consistency for the single-body meteor theory applied to these very small meteoroid masses. A simple explanation for this consistency might be that fragmentation in the ablation process is not significant for these very small meteoroids.

The RCS of the meteor, which represents the reflection coefficient from the meteor plasma, will be maximized when the meteor achieves the best balance between the electron plasma density and the radius of the meteor head. At high altitudes, the meteor head plasma has a large radius but is more diffuse, similar to meteor trails, so the reflection coefficient will be small. At low altitudes, the plasma density will be high but the highly collisional atmosphere spatially restricts the meteor head plasma size so the reflection coefficient is again small. For the mass and velocity range detected by ALTAIR, the meteors show the best balance between

Fig. 7. (a) Maximum electron line density derived from the three-equation ablation model and (b) maximum electron line density from ALTAIR head echo observations. In contrast to Fig. 6, these data are all plotted as a function of height above Earth and meteor velocity.

plasma density and meteor plasma size at approximately 103 km altitude, which give the largest reflection. This qualitative description assumes the meteor is traveling “directly toward” the radar. Using this geometry, the observed meteor head plasma appears spherically distributed. Off axis meteor head observations are on non-spherically distributed plasma that establishes another level of complexity with regard to its scattering characteristics and is not considered here. We assume the diffuse upper limit and the constrained lower limit affect the ability of high-gain radar to detect meteor head plasma. The modeling of the dependence of this effect on observing meteor head echoes is left for future work. This head echo observation artifact is similar to the meteor ceiling bias experienced by specular meteor trail radars.

## 6. Bias correction

The dependence of ionization on the initial meteoroid mass and velocity must be addressed to estimate the absolute number of meteoroids at Earth as a function of velocity. The removal of the mass dependence is problematic since we do not know the mass of each meteoroid a priori. Therefore, a lower limit for the minimum detectable mass for each velocity (bin) is calculated and is then normalized on the basis of ALTAIR’s minimum sensitivity. For the sake of comparison, the HRMP minimum detectable mass at  $30 \text{ km s}^{-1}$  is  $10^{-4}$  g and for ALTAIR VHF it is  $10^{-6}$  g.

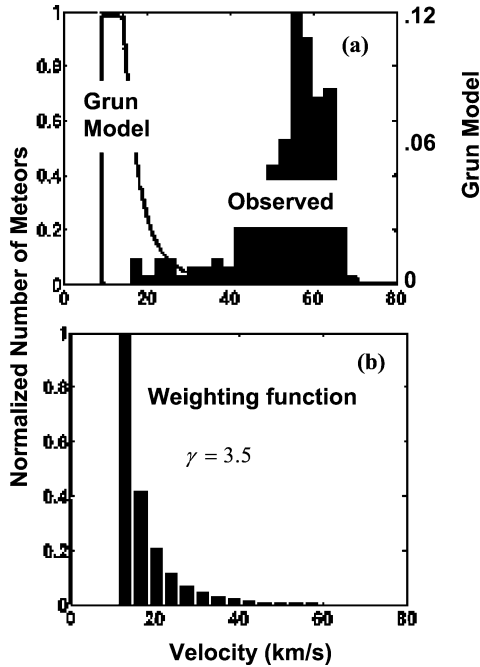


Fig. 8. Normalized number of meteors observed at earth as a function of velocity according to the Grun interplanetary model (1985) plotted with ALTAIR observations (a). The ALTAIR UHF observations, (a), are normalized to ALTAIR’s minimum detectable mass,  $M_{60}$  ( $10^{-8}$  g), at  $60 \text{ km s}^{-1}$ . The second panel, (b), graphically illustrates the weighting function for the dependence of the ionization efficiency on velocity.

Given the estimate for the minimum detectable VHF radio magnitude,  $M$ , for the ALTAIR system of +11, the minimum detectable mass (in grams) at a particular velocity can be calculated using (Verniani, 1973):

$$m_{\min} = (35.8 - 9.8 \log V_0 - M)/2.3, \quad (7)$$

where  $V_0$  is the initial meteor velocity ( $\text{m s}^{-1}$ ). Verniani (1973) derived the relation theoretically and subsequently

modified the relation through the analysis of 5759 faint radio meteors. Verniani’s semi-empirical result is used here and was derived for meteoroids in the observed mass range of  $10^{-6} \text{ g} \leq m \leq 10^{-2} \text{ g}$ , with median masses near  $10^{-4} \text{ g}$ . Comparing the observed velocity distribution measured by ALTAIR (Fig. 8) and the Grun interplanetary meteoroid model (1985) illustrates the strong observational velocity bias.

For example, to remove the observational dependence on mass and velocity, we first normalize the observations to ALTAIR’s minimum detectable mass at  $60 \text{ km s}^{-1}$  to  $m_{60} = 9.7 \times 10^{-8} \text{ g}$ . We selected  $60 \text{ km s}^{-1}$  since this is where the peak of the north apex velocity distribution resides.

Following Taylor (1995), the number of meteors observed in a particular velocity bin is  $N(m > m_V)$ , where the minimum detectable mass at that velocity is  $m_V$ . The normalized number of meteors with a velocity greater than the detection threshold at  $60 \text{ km s}^{-1}$  is

$$N(m > m_{60}) = \left(\frac{m_{60}}{m_V}\right)^{-\alpha} N(m > m_V). \quad (8)$$

The cumulative mass index  $\alpha$  (slope of the meteoroid particle distribution function) is set equal to 1.6 (Grun et al., 1985). The application of a normalized velocity weighting function

$$W = \left(\frac{V_{\text{bin}}}{V_{\min}}\right)^{-\gamma} \quad (9)$$

to each velocity bin corrects for the velocity bias.  $V_{\text{bin}}$  is the velocity of each bin spanning  $11 \text{ km s}^{-1} \leq V \leq 72 \text{ km s}^{-1}$ ;  $V_{\min}$  is the value of the smallest velocity bin and therefore normalizes  $W$ .  $\gamma$  is the exponent of the velocity factor from the ionization efficiency shown in Eq. (6).

Figure 9 illustrates the bias corrected and observed fraction of meteors versus velocity from the HRMP and ALTAIR. The ALTAIR and HRMP data show an observed peak

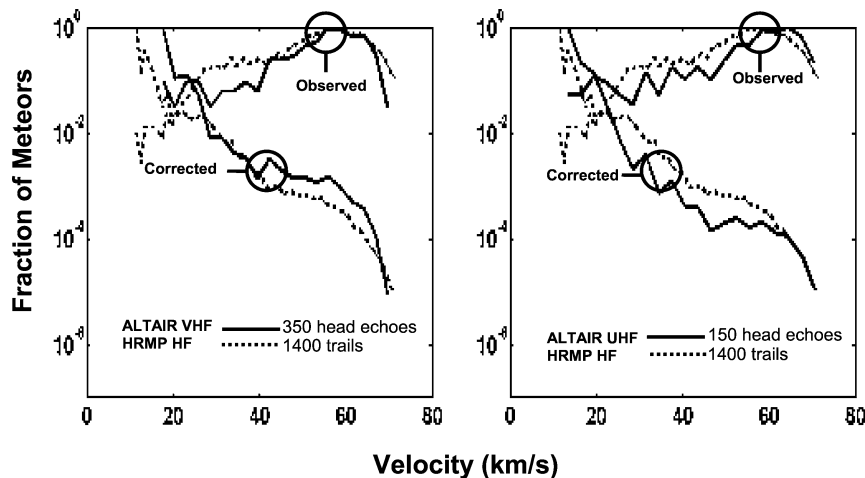


Fig. 9. Fractional number of meteors versus observed velocity from the HRMP study and ALTAIR. The HRMP and ALTAIR North Apex data show a peak velocity near  $56 \text{ km s}^{-1}$ . After the removal of the estimate for the velocity selection effect, the two distributions show similar characteristics and are in relatively good agreement, though differences in absolute numbers at lower velocities are apparent. We attribute this deviation (particularly at lower velocities) to the statistics of the HRMP data that are much better than the ALTAIR head echo data (as evidenced by the ‘choppy’ ALTAIR normalized curve in places).

velocity near  $56 \text{ km s}^{-1}$ . After bias correction, the two distributions remain in relatively good agreement. There is almost no sampling of the lower velocity population from the helion/anti-helion source in the ALTAIR dataset. Future high-power radar observations will sample these sporadic radiants and provide a more uniform directional sampling.

## Acknowledgments

The authors gratefully acknowledge support received from the military and civilian staff at the US Army Reagan Test Site during the 1998 meteor shower. MIT Lincoln Laboratory's Aerospace and Ballistic Missile Defense Divisions including Dr. Ken Roth, Chris Moulton, Dr. Ramaswamy Sridharan and Kurt Schwan supported the analysis shown here. Cheryl Nunes provided invaluable editorial support in the preparation of this manuscript. This was all prepared for the Department of the Army under Air Force Contract F19628-00-C-0002. Opinions, interpretations, conclusions, and recommendations are those of the authors and are not necessarily endorsed by the US Air Force or Army. This material is also partially based on work supported by the National Science Foundation under grant number ATM-9986976.

## References

- Baggaley, W.J., Bennet, R.G.T., Steel, D.I., Taylor, A.D., 1994. The Advanced Meteor Orbit Radar facility: AMOR. *Quart. J. Roy. Astron. Soc.* 35, 293–320.
- Baggaley, W.J., Bennet, R.G.T., Taylor, A.D., 1997. Radar meteor atmospheric speeds determined from echo profile measurements. *Planet. Space Sci.* 45 (5), 577–583.
- Bronshten, V.A., 1983. *Physics of Meteoric Phenomena*. Reidel, Dordrecht.
- Brown, P., Jones, J., 1995. A determination of the strengths of the sporadic radiometer sources. *Earth Moon Planets* 68, 223–245.
- Brown, P., Hunt, S., Close, S., 2001. Astronomical and physical data for meteoroids recorded by the ALTAIR radar. In: Warmbein, B. (Ed.), *Proc. Meteoroids 2001 Conf.*, Kiruna, Sweden, Noordwijk. In: ESA SP, Vol. 495, pp. 469–474.
- Cepelcha, Z., Borovicka, J., Elford, W.G., Revelle, D.O., Hawkes, R.L., Porubcan, V., Simek, M., 1998. Meteor phenomena and bodies. *Space Sci. Rev.* 84 (3–4).
- Close, S., Hunt, S., Minardi, M., McKeen, F., 2000. Analysis of Perseid meteor head echo data collected using the Advanced Research Projects Agency Long-Range Tracking and Instrumentation Radar (ALTAIR). *Radio Sci.* 35, 1233–1240.
- Close, S., Hunt, S., Oppenheim, M., McKeen, F., 2001. Simultaneous dual-frequency observations of meteor head echoes using ALTAIR. In: *Proceedings Third European Conference on Space Debris*.
- Close, S., Oppenheim, M., Hunt, S., Coster, A.J., 2003. Full-wave solutions developed for scattering from meteor head echo plasma to determine head plasma density and meteoroid mass. *Icarus*. Submitted for publication.
- Coster, A.J., Gaposhkin, E.M., Thornton, L.E., 1992. Real-time ionospheric monitoring system using GPS. *J. Inst. Navig.* 39 (2), 191–204.
- Grebowski, J.M., 1981. Meteoric ion production near Jupiter. *J. Geophys. Res.* 86 (A3), 1537–1543.
- Grun, E., Zook, H.A., Fichtig, H., Giese, R.H., 1985. Collisional balance of the meteoroid complex. *Icarus* 62, 244–272.
- Hawkins, G.S., 1956. Meteor ionization and its dependence on velocity. *Smithsonian Contributions to Astrophysics*.
- Hawkins, G.S., 1963. The Harvard Radio Meteor Project. *Smithsonian Contributions to Astrophysics* 7, 53.
- Hawkins, G.S., Southworth, R.B., Verniani, F., 1964. On the Ablation coefficient of meteors. Harvard Radio Meteor Project. Research Report No. 10.
- Hedin, A.E., 1983. A revised thermospheric model based on Mass Spectrometer and Incoherent Scatter data: MSIS-83. *J. Geophys. Res.* 88, 10170.
- Hedin, A.E., 1987. MSIS-86 thermospheric model. *J. Geophys. Res.* 92, 4649.
- Hedin, A.E., 1991. Extension of the MSIS thermosphere model into the middle and lower atmosphere. *J. Geophys. Res.* 96, 1159.
- Herlofson, N., 1948. The theory of meteor ionization. *Rep. Prog. Phys.* 11, 444.
- Hey, J.S., Parsons, S.J., Stewart, G.S., 1947. Radar Observations of the Gicobinid Meteor Shower. *Mon. Not. R. Astron. Soc.* 107, 176–183.
- Hunt, S., Close, S., Coster, A., Stevens, E., Schuett, L., Vardaro, A., 2000. Equatorial atmospheric and ionospheric modeling at Kwajalein missile range. *MIT Lincoln Lab. J.* 12 (1).
- Hunt, S., Close, S., Oppenheim, M., Dyrud, L., 2001. Two-frequency meteor observations using the Advanced Research Project Agency Long-Range Tracking and Instrumentation Radar (ALTAIR). In: *ESA—Proc. of the Meteoroids 2001 Conf.*, pp. 451–455.
- Janches, D., Mathews, J.D., Meisel, D.D., Zhou, Q.H., 2000a. Micrometeor observations using the Arecibo 430 MHz radar. I. Determination of the ballistic parameter from measured Doppler velocity and deceleration results. *Icarus* 145, 53–63.
- Janches, D., Mathews, J.D., Meisel, D.D., Getman, V.S., Zhou, Q., 2000b. Doppler studies of near-Antapex UHF radar micrometeors. *Icarus* 143, 347–353.
- Jones, J., Brown, P., 1993. Sporadic meteor radiant distributions: orbital survey results. *Mon. Not. R. Astron. Soc.* 265, 524–532.
- Jones, W., 1997. Theoretical and observational determinations of the ionization coefficient of meteors. *Mon. Not. R. Astron. Soc.* 288, 995–1003.
- Lebedinets, V.N., 1973. Evolutionary and Physical Properties of Meteoroids. In: *Proceedings of IAU Colloq. 13th*, Albany, NY, 14–17 June 1971. In: *NASA SP*, Vol. 319, p. 259.
- Massey, H.S., Sida, D.W., 1955. Collision processes in meteor trails. *Phil. Mag.* 46, 190–198.
- Mathews, J.D., Meisel, D.D., Hunter, K.P., Getman, V.S., Zhou, Q., 1997. Very high resolution studies of micrometeors using the Arecibo 430 MHz radar. *Icarus* 126, 157–169.
- Opik, E.J., 1958. *Physics of Meteor Flight in the Atmosphere*. Interscience, New York.
- Pellinen-Wannberg, A., Wannberg, G., 1994. Meteor observations with the European incoherent scatter UHF radar. *J. Geophys. Res.* 99, 11379–11390.
- Skolnick, M.I., 1980. *Introduction to Radar Systems*. McGraw-Hill.
- Taylor, A.D., 1995. The Harvard radio meteor project velocity distribution reappraised. *Icarus* 116, 154–158.
- Taylor, A.D., 1997. The radiant distribution of meteoroids encountering the Earth. *Adv. Space Res.* 20 (8), 1505–1508.
- Taylor, A.D., 1998. Meteor orbital element distribution at 1 AU deduced from the Harvard Radio Meteor Project observations. *Earth Planets Space* 50, 569–575.
- Verniani, F., 1973. An analysis of the physical parameters of 5759 faint radio meteors. *J. Geophys. Res.* 78 (35).
- Whipple, F.L., 1950. The theory of micro-meteorites. Part I. In an isothermal atmosphere. *Proc. Nat. Acad. Sci. USA* 36 (12), 687–695.
- Whipple, F.L., 1951. The theory of micro-meteorites. Part II. In heterothermal atmospheres. *Proc. Nat. Acad. Sci. USA* 37 (1), 19–30.
- Whipple, F.L., 1966. Final scientific report, Harvard Radio Meteor Project. *Smithsonian Astrophysical Observatory report*. Nasa CR-158.
- Zhou, Q.-H., Perillat, P., Cho, J.Y.N., Mathews, J.D., 1998. Simultaneous meteor echo observations by large aperture VHF and UHF radars. *Radio Sci.* 33, 1641–1654.